IEEE Access
Multidisciplinary : Rapid Review : Open Access Journal

Received August 14, 2019, accepted August 24, 2019, date of publication August 29, 2019, date of current version September 12, 2019.

Digital Object Identifier 10.1109/ACCESS.2019.2938199

Sensorless-Based Active Disturbance Rejection Control for a Wind Energy Conversion System With Permanent Magnet Synchronous Generator

SHENGQUAN LI[1], MENGYING CAO[1,2], JUAN LI[1], JIUFA CAO[1], AND ZHONGWEI LIN[3]

[1]School of Electrical, Energy and Power Engineering, Yangzhou University, Yangzhou 225127, China
[2]School of Automation, Southeast University, Nanjing 210096, China
[3]State Key Laboratory of Alternate Electrical Power System with Renewable Energy Sources, School of Control and Computer Engineering, North China Electric Power University, Beijing 102206, China

Corresponding author: Shengquan Li (sqli@yzu.edu.cn)

This work was supported in part by the National Natural Science Foundation of China under Grant 61903322 and Grant 61773335, in part by the Natural Science Foundation of Jiangsu Province under Grant BK20171289 and Grant BK20160476, in part by the Six Talent Peaks Foundation of Jiangsu Provincial under Grant KTHY2018038, in part by the Natural Science Foundation of Yangzhou City for Outstanding Young Scholars under Grant YZ2017099, and in part by the State Key Laboratory of Alternate Electrical Power System with Renewable Energy Sources under Grant LAPS19003.

ABSTRACT This paper focuses on the control problem of wind energy conversion systems (WECSs) with direct-driven permanent magnet synchronous generator (PMSG) working in variable power output stage. A novel compound control scheme combined the active disturbance rejection controller (ADRC) and speed sensorless technology is proposed. In order to achieve maximum power point tracking (MPPT), a speed control loop is designed based on ADRC to improve the speed tracking ability and anti-disturbance ability of system. Moreover, considering the large amount of system model information, a model-assisted ADRC is designed on the nominal ADRC to improve the response speed of system and reduce the energy consumption for the system control. Additionally, to solve the contradiction between the requirement of speed sensor precision and the economy of system design, a speed observer based on current model is designed in $\alpha - \beta$ coordinate system. Furthermore, a resistance observer is introduced to improve the convergence rate of the observer. And a position sensorless observer structure based on the speed observer is proposed. Finally, simulation studies are conducted to evaluate power tracking performances of the proposed speed-observer-based model assisted ADRC technology. It is shown that the proposed compound scheme exhibits significant improvements in both control performance and anti-disturbance ability with high observation precision compared with the normal ADRC method.

INDEX TERMS Active disturbance rejection control (ADRC), wind energy conversion system (WECS), permanent magnet synchronous generator (PMSG), speed observer, sensorless.

I. INTRODUCTION

Considering limitation of fossil energy and negative impact on environment caused by fossil fuel emissions, increasing demand for energy has gradually turned our attention to renewable energy generation, which involves control of generator sets [1]–[3]. The direct-driven PMSG has been widely applied in variable wind turbine applications, since it owns some competitive advantages, such as gearless construction, high power density, little noise, high efficiency, and excellent reliability [4]–[8]. In order to reduce the damage to mechanical structure of system caused by drastic changes of wind speed, WECSs subjected to severe natural wind are controlled to track maximum power point and improve stability of WECS. Furthermore, the limits of mechanical and electrical characteristics of WECSs on rated output power of generator can be relaxed, and rated capacity of generators can be increased effectively.

To control active and reactive power of PMSG based WECSs, different control methods are proposed for the challenges of various disturbances and limitation of system operation, such as unknown external disturbances, time-varying and unpredictability of wind speed, nonlinearity and strong coupling of PMSG, saturation of the electrical components, bearing capacity of mechanical structures and

The associate editor coordinating the review of this article and approving it for publication was Yan-Jun Liu.

so on [1], [5], [6]. Thus, to obtain the satisfactory control performance for the PMSG-based WECSs, a high-power-tracking-performance of these systems is required to have an excellence disturbance rejection ability. Over the past decades, numerous control strategies have been applied to track the maximum power from the wind turbine equipped with PMSG [9]–[16].

Nonlinear control methods are regards as natural choices, since many kinds of nonlinear controllers have been employed to the PMSG based WESCs, such as, decoupled d-q vector controller[9], [10], neural network method [11], [12], robust control[13], nonlinear feedback control [14], model predictive control (MPC) method [15], backstepping control strategy [16] etc. A novel direct-current vector control technique based on the transient and steady-state models of PMSG is introduced by integrating fuzzy, adaptive and traditional PID control technologies in ref. [9]. A universal controller is further proposed to regulate tracking error in ref. [10] by combining adaptive method, intelligent control method, robust differentiator techniques. In refs. [11], [12], a novel RBF neural network methods employed on-line training methods and cloud model are proposed to extract maximum power for the optimal control of PMSG-based WECSs. In ref. [13], a novel H_∞ based robust control system is designed for effective control of active and reactive power flow between WECS and grid, which provides a strategy for efficient grid connection of WECS. A nonlinear feedback control scheme for the grid side converter of PMSG-based wind turbine system is proposed to deal with the network disturbance in ref. [14]. Considering the disturbances caused by load and uncertain wind speed, as well as changes of system parameters, a frequency regulation strategy based on MPC is presented to generate torque compensation in ref. [15]. An adaptive backstepping control system is designed to compensate the parameter uncertainties of a variable-speed wind energy conversion system with PMSG in ref. [16]. Although these methods can improve the power tracking performance of PMSG based WECSs, they are really hard to reject the internal and external disturbances, simultaneously and directly. Sliding mode control method (SMC) is employed as one of the most attractive nonlinear controllers used in PMSG based WECSs, since this kind of nonlinear control strategies own excellent anti-disturbances ability. In ref. [17], a sliding-mode control based on a modified reaching law is proposed to control WECS, and a new structure of interface between the wind turbine and grid is introduced to increase the practicability and economy of WECS control. In order to avoid the chattering phenomenon of the traditional first order SMC, a high-order SMC is proposed to track the maximum power of PMSG-based WECS in ref. [18]. However, the chattering phenomena and reaching phase stability problem are still the main problems for the industrial applications.

The higher and higher requirement on system tracking performance has motivated various researchers to improve the control performance by designing the controller directly against the disturbances. Recently, two kinds of significant disturbance estimate methods have been proposed to reject the undesirable influences of wind speed and model parameter uncertainties. One is the disturbance observer-based control (DOBC), originally proposed by Ohnishi *et al.* [19]. In ref. [20], the observed disturbance torque is feed-forward to improve the maximum power tracking performance of the PMSG systems. DOBC scheme has also been proved to be effective in reducing the effects of model uncertainty of PMSG-based wind turbine system [21]. In ref. [22], in order to estimate the perturbations caused by parameter variations of the PMSG or by any ummodeled dynamics, a disturbance observer with simple structure is proposed to enhance the feedback controller. Considering the model-plant mismatches and severe load torque variation, a disturbance observer is designed to improve the power tracking performance for the PMSG-based wind power generation systems [23]. Focusing on these research results, DOBC has been proved to effective in reducing the effects of the internal or external disturbances in PMSG-based WECSs by compensating them from the feed-forward channel. The major advantage of the DOBC is that the anti-disturbance ability of closed-loop system is improved without reducing the normal control performance [24].

Another kind of disturbance estimation concept is the extended state observer (ESO) originally proposed by Han in 1995 [25]. In the absence of a detailed mathematical model, it also can regard the internal and external disturbances as a new state of system which can be dynamically compensated by feed-forward channel. Thus, it shows potential ability to deal with the dynamic and environmental uncertainties, nonlinearities, parametric variations, coupling effects, etc. Owing to such promising features, the ESO-based control structure also called active disturbance rejection control has been fully articulated in 2009 [26]. On the basis of Han's nonlinear ADRC, a novel structure of linear active disturbance rejection control (LADCR) is further proposed by Gao to simplify the controller design and reduce the difficulty in parametric tuning [27]. Furthermore, this maximum power point tracking (MPPT) control strategy has a few tuning parameters, which makes it easy to be implemented in the real system, so the LADRC method has also been applied to wind energy conversion systems [4], [28]–[37]. Since the external and internal disturbances can be compensated as an extended state of the whole system in these references, ADRC-based control methods can enhance the dynamic performance of PMSG based WECSs. However, this would require additional mechanical sensors and cumbersome computations, which increase the cost and the encumbrance of the generator.

For the aim of maximum power point tracking (MPPT), sensors with high sensitivity are usually used to monitor the natural wind in real time. Although velocity is theoretically a differential of the angle, it is easy to introduce noise signals to the angular differential. So one may wish that the control algorithm for WECS do not require any mechanical speed sensor [20], [21], [38]–[40]. In ref. [38], an original sensorless-based MPPT strategy with speed estimation method is proposed to improve the tracking performance of PMSG. In ref. [39], a control scheme combined the model-prediction control and speed sensorless control is proposed for starting rotating induction motor with the convergence condition of speed estimation deduced. In ref. [40], a derivative-free nonlinear Kalman filtering method is proposed to control the distributed PMSGs without speed sensor. Furthermore, an improved control scheme is proposed by redesigning the filter as a disturbance observer to estimate the uncertainties of the system. So as discussed above, aiming to improve the power tracking performance of the PMSG-based WECSs with various uncertainties, an ADRC based MPPT control method with sensorless technology, is developed to completely attenuate the internal and external disturbances in this paper.

This paper is organized as follows. **Section II**gives description of the system dynamic model. A novel structure of the ADRC based on a speed observer technology for a PMSG-based WECS is introduced in **Section III**. And the design process and conversion analysis of the proposed speed observer strategy are also discussed in this section. In **Section IV**, numerical simulation results based on several wind types will show the effectiveness of the proposed control strategy. Finally, the conclusions end the paper.

II. DYNAMIC CHARACTERISTICS OF WIND TURBINE AND CHALLENGES FOR CONTROL DESIGN

Wind power system can be roughly divided into two parts: wind turbine with generator and load side. Wind turbine includes wind wheel (part that captures wind energy and converts to mechanical energy) and generator (part that converts mechanical energy from wind turbines into electric energy). The load side includes frequency converters, transformers, electrical equipment and other power consuming components on the grid.

A. DYNAMIC CHARACTERISTICS OF WIND WHEEL

According to Bates' law, the wind turbine output mechanical torque can be expressed as follows [40]:

$$T_{tur} = \frac{1}{2}\rho\pi R^3 C_p(\lambda, \beta)\, v^2 \tag{1}$$

in which

$$\begin{cases} C_p(\lambda, \beta) = 0.5176(\dfrac{116}{\gamma} - 0.4\beta - 5)e^{-\frac{21}{\gamma}} + 0.0068\lambda \\ \dfrac{1}{\gamma} = \dfrac{1}{\lambda + 0.08\beta} - \dfrac{0.035}{\beta^3 + 1} \end{cases} \tag{2}$$

In Eq. (1), mechanical power output from the wind turbine is expressed by $P_{tur}(W)$, air density is expressed by $\rho\,(kg/m^3)$, airflow velocity is expressed by $v\,(m/s)$, wind energy utilization coefficient is expressed by $C_p(\lambda, \beta)$ which is a nonlinear function of β and λ, the tip-speed ratio is expressed by λ which is the ratio of tip circumferential velocity to airflow velocity, and the pitch angle is expressed by $\beta\,(°)$ which is the angle between the blade chord and the rotating plane, respectively.

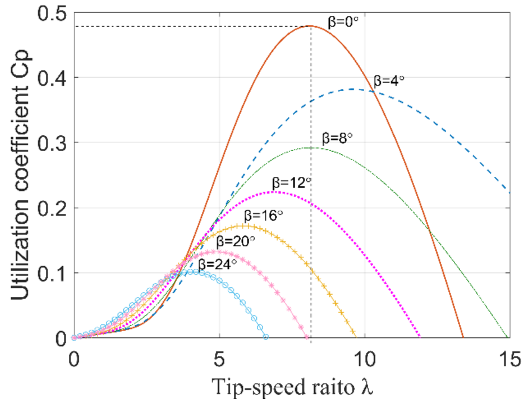

FIGURE 1. The curves of wind energy utilization.

In fact, the parameter $C_p(\lambda, \beta)$ is a cluster of curves at different pitch angles. According to Eq. (2), a cluster of $C_p(\lambda, \beta)$ can be obtained, as shown in Fig.1. Obviously, with a smaller pitch angle β, the peak value of wind energy utilization coefficient curve is greater. In particular, the optimal tip speed ratio is $\lambda_{opt} = 8.1$ when $\beta = 0°$.

The desired speed $\omega_r(rad/s)$ of wind turbine can be calculated according to the optimal tip speed ratio λ_{opt} through the following equation.

$$\omega_r = \frac{v \cdot \lambda_{opt}}{R} \tag{3}$$

In addition, the aerodynamic torque $T_{tur}\,(N \cdot m)$ of wind wheel can be obtained by following Eq. (4).

$$T_{tur} = \frac{P_{tur}}{\omega} = \frac{1}{2} \cdot \frac{\rho\pi R^5 C_p(\lambda, \beta)}{\lambda_{opt}^3} \cdot \omega^2 \tag{4}$$

The mechanical speed of the wind turbine is expressed by $\omega\,(rad/s)$ in Eq. (4).

B. DYNAMIC CHARACTERISTICS OF PMSG

Voltage model of PMSG in $\alpha-\beta$ coordinate system as following Eq. (5) can be contained by Clarke transformation with the voltage model in $A-B-C$ coordinate system [4], [28].

$$\begin{bmatrix} u_\alpha \\ u_\beta \end{bmatrix} = \begin{bmatrix} R_s & 0 \\ 0 & R_s \end{bmatrix} \begin{bmatrix} i_\alpha \\ i_\beta \end{bmatrix} + \begin{bmatrix} \dot{\psi}_\alpha \\ \dot{\psi}_\beta \end{bmatrix} \tag{5}$$

where $\begin{bmatrix} \psi_\alpha \\ \psi_\beta \end{bmatrix} = \begin{bmatrix} L & 0 \\ 0 & L \end{bmatrix} \begin{bmatrix} i_\alpha \\ i_\beta \end{bmatrix} + \psi_f \begin{bmatrix} \cos(n_p\theta) \\ \sin(n_p\theta) \end{bmatrix}$.

In Eq. (5), u_α and u_β are projections of stator voltage on α and β axes (V), i_α and i_β are projections of stator current on α and β axes (A), ψ_α and ψ_β are projections of stator flux linkage on α and β axes (Wb), R_s represents stator resistance (Ω), L represents stator inductance (H), ψ_f is rotor flux linkage (Wb), n_p represents pole pairs of PMSG, and θ represents rotor mechanical angle (rad), respectively.

The electromagnetic torque $T_e\,(N \cdot m)$ in $\alpha-\beta$ coordinate system can be expressed as follows.

$$T_e = \frac{3}{2} n_p \psi_f\, [i_\beta \cos(n_p\theta) - i_\alpha \sin(n_p\theta)] \tag{6}$$

Through Park transformation, the voltage model of PMSG in $\alpha-\beta$ coordinate system can be transformed into the voltage model in $d-q$ coordinate as follows.

$$\begin{bmatrix} u_d \\ u_q \end{bmatrix} = \begin{bmatrix} R_s & -n_p\omega L \\ n_p\omega L & R_s \end{bmatrix} \begin{bmatrix} i_d \\ i_q \end{bmatrix} + \begin{bmatrix} L & 0 \\ 0 & L \end{bmatrix} \begin{bmatrix} \dot{i}_d \\ \dot{i}_q \end{bmatrix} + n_p\omega\psi_f \begin{bmatrix} 0 \\ 1 \end{bmatrix} \tag{7}$$

where u_d, u_q, i_d and i_q are the projections of stator voltage on d and q axes (V), and the projections of stator current on d and q axes (A), respectively.

The electromagnetic torque T_e in $d-q$ coordinate system can be defined as follows.

$$T_e = \frac{3}{2} n\psi_f i_q \tag{8}$$

In addition, the dynamics of wind turbine shaft can be expressed by Eq. (9).

$$J\frac{d\omega}{dt} = T_{tur} - T_e - B\omega \tag{9}$$

where system inertia of wind turbine is expressed by $J\left(kg\cdot \mathrm{m}^2\right)$ and viscous damping is expressed by $B\left(kg\cdot m^2/\mathrm{s}\right)$.

C. THE CONTROL DESIGN CHALLENGES

As discussed above, the direct driven PMSG-based WECS is a complex system with serious internal and external disturbances, such as uncertainty wind speeds, model error, nonlinear aerodynamic torque, multivariable coupling, etc. The main challenge is how to attenuate the effect of the internal and external disturbances while achieving excellent maximum power capturing performance. So it is significant to design a controller being independent of accurate mathematical model and strong anti-disturbance ability. Considering the features of ESO method, the ADRC-based MPPT strategy is proposed to observer the internal and external disturbances. Moreover, the satisfactory power tracking performance can be obtained in the absence of the model of the wind turbine only with the system order as a prior. Additionally, in order to reduce the estimation burden of the extended state observer, the model information estimated by inertia and torque observer, is introduced into the ADRC to further improve the response speed of the speed controller and the stability of the system. Besides, the measurement of stator current and stator voltage is relatively easy, and the technology of avoiding magnetoelectric field interference is relatively perfect. Therefore, the speed sensorless controller based on an observer technology is proposed for wind power control system. Considering these problems related to PMSG-based WECS, the proposed model assisted ADRC-based on sensorless technology is an effective controller in dealing with problems of the disturbances and physical velocity sensor in wind turbine and tracking the maximum wind power.

III. COMPOUND CONTROL SCHEMES BASED ON ADRC

A. MODEL-ASSISTED ADRC DESIGN FOR PMSG

The structure of control scheme based on model-assisted ADRC for WECS is shown in Fig.2. The outer loop is the speed loop, and the inner loop is the current loop. The speed observation signal $\hat{\omega}$ output from the speed observer is used to instead of the detection value of the generator speed sensor to provide the speed signal for the speed controller based on ADRC.

According to Eq.3, the desired speed ω_r of the wind turbine based on the optimal tip-speed ratio λ_{opt} can be obtained. Furthermore, maximum power point can be tracked by adjusting the wind turbine speed in real time according to ω_r. In this paper, speed controllers based on ADRC are chosen to track the desired speed. Based on the real-time speed of generator ω, the lumped disturbance of the system is estimated nearly accurately by the extended state observer (ESO). Meanwhile, the control variable $u_0(t)$ is calculated based on the difference between ω_r and $\hat{\omega}$ by the state error feedback (SEF) part. Besides, the feed-forward part of controller is designed to restrain the influence of the lumped disturbance $a_0(t)$ on the state quantity of the system.

Traditional PI control is widely used in practice because of its simple structure and easy realization. Moreover, as measurable states of the generator, the stator currents i_d and i_q can not only reflect the station of the generator, but also affect the electromagnetic torque of the generator T_e effectively. Therefore, the current loop based on PI control is designed in this paper.

It can be seen from Eq. (7) to Eq. (9) that i_q participates in the whole mathematical model construction of PMSG in $d-q$ coordinate system. In other words, i_q contains the most information. Therefore, i_{qr} is chosen as a key variable to connect the speed loop and the current loop, which is not only the output control variable $u(t)$ of the speed loop, but also the desired current input of the current loop on q axis.

Cross-coupling voltages are defined as Eq. (10).

$$\begin{aligned} u_q^* &= n_p\omega L_2 i_q \\ u_d^* &= n_p\omega L_2 i_d + n_p\omega\psi_f \end{aligned} \tag{10}$$

From Eq. (7), it can be seen that u_d and u_q are not only related to i_d and i_q, but also affected by the cross-coupling voltage. When $i_d = i_{dr} = 0$, the desired value of u_d should be $u'_{dr} = -u^*_{qr}$ instead of zero. Therefore, after adjusting the current, the cross-coupling voltage is compensated on voltages u_{dr} and u_{qr} output of PI controller, and the final desired voltages u'_{dr} and $u'_{qr}$are obtained. Furthermore, the desired voltages $u_{\alpha r}$ and $u_{\beta r}$ in $\alpha-\beta$ coordinate system can be transformed from u'_{dr} and u'_{qr} by inverse park transformation.

In fact, wind turbine of WECS acts as a non-ideal source in a circuit so that the generator stator voltage can be tracked by adjusting the dummy load, which can be achieved based

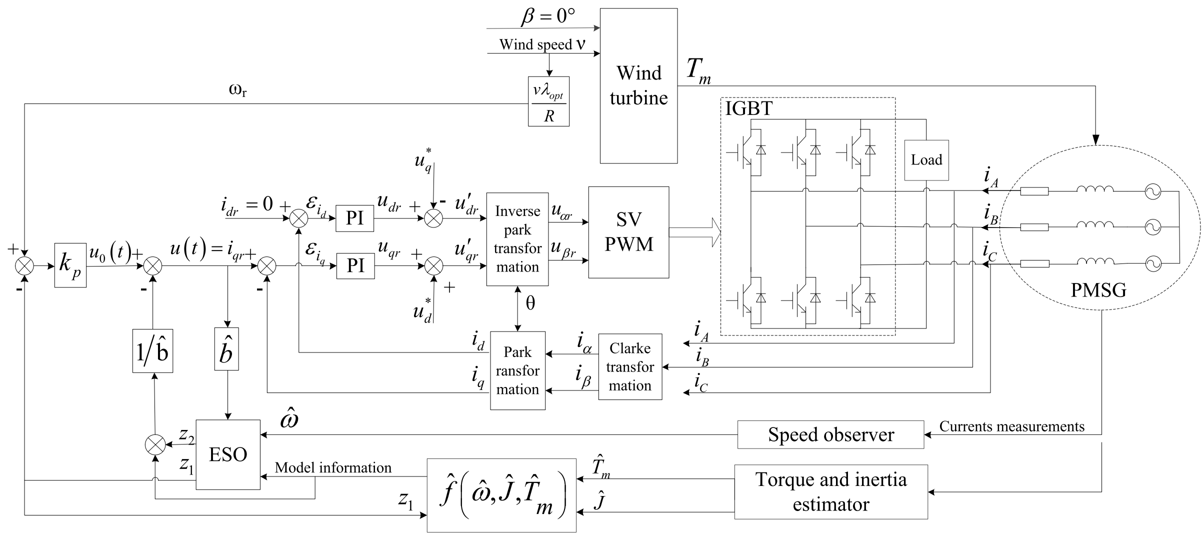

FIGURE 2. **The structure of control scheme based on model-assisted ADRC for WECS.**

on $u_{\alpha r}$ and $u_{\beta r}$ by the space vector pulse width modulation (SVPWM) technology [41], [42]. When the voltages of generator stator are desired voltages, the stator currents are desired currents, and the corresponding speed of generator is desired speed.

B. SPEED OBSERVER DESIGN FOR PMSG

Although rotational speed is theoretically the differential of electrical angle, it is easy to introduce noise signal by using differential of position signal as speed observation value, so closed-loop observer is designed in this paper to improve the accuracy of speed observation.

The d-q axes have the same speed with generator rotor, commonly. To put it another way, the transformation from $\alpha-\beta$ coordinate system to d-q coordinate system requires information of rotor speed to determine the position of d and q axes. Fortunately, the Clarke transformation of currents in $A-B-C$ coordinate system requires only rotor position signal. Therefore, the speed observer is designed based on the current model of PMSG in $\alpha-\beta$ coordinate system.

According to Eqs. (1) ~ (6) and (9), the state space model of PMSG can be expressed by the following form.

$$\begin{cases} \dot{x} = Ax + U \\ y = Cx \end{cases} \tag{11}$$

where $A = \begin{bmatrix} -R_s/L & 0 & k_{fs}/L \\ 0 & -R_s/L & -k_{fc}/L \\ 3k_{fs}/2J & -3k_{fc}/2J & (k_t\omega - B)/J \end{bmatrix}$, $x = \begin{bmatrix} i_\alpha \\ i_\beta \\ \omega \end{bmatrix}$, $U = \begin{bmatrix} u_\alpha/L \\ u_\beta/L \\ 0 \end{bmatrix}$, and $C = \begin{bmatrix} 1 & 0 & 0 \\ 0 & 1 & 0 \end{bmatrix}$.

In addition, $k_{fc} = n_p\psi_f \cos(n_p\theta)$, $k_{fs} = n_p\psi_f \sin(n_p\theta)$, and $k_t = \rho\pi R^5 C_p(\lambda, \beta)/2\lambda^3$.

The matrix Q_o is defined as follows.

$$Q_o = \begin{bmatrix} C & CA & CA^2 \end{bmatrix}^T = \begin{bmatrix} 1 & 0 & 0 \\ 0 & 1 & 0 \\ -R_s/L & 0 & k_{fs}/L \\ 0 & -R_s/L & -k_{fc}/L \\ \frac{R_s^2}{L^2} + \frac{3k_{fs}^2}{2JL} & -\frac{3k_{fs}k_{fc}}{2JL} & k_{fs}k_{tb1} \\ -\frac{3k_{fc}k_{fs}}{2JL} & \frac{R_s^2}{L^2} + \frac{3k_{fc}^2}{2JL} & k_{fc}k_{tb2} \end{bmatrix} \tag{12}$$

With $k_{tb1} = -\frac{R_s}{L^2} + \frac{k_t\omega - B}{JL}$ and $k_{tb2} = \frac{R_s}{L^2} + \frac{k_t\omega - B}{JL}$.

Since k_{fc} and k_{fs} will not be zero at the same time in practice, it can be concluded that $rank(Q_o) = 3$. Therefore, the speed of the generator can be observed.

The mathematical model of wind turbine dynamics in $\alpha-\beta$ coordinate system can be further obtained as following Eq. (13), according to Eq. (6) and Eq. (9).

$$\dot{\omega} = \frac{1}{J}\left(T_{tur} - \frac{3}{2}n_p\psi_f I_{\alpha\beta} - B\omega\right) \tag{13}$$

with $I_{\alpha\beta} = i_\beta \cos(n_p\theta) - i_\alpha \sin(n_p\theta)$. So the observer equation can be obtained by the following Eq. (14).

$$\dot{\hat{\omega}} = \frac{1}{J}\left(T_{tur} - \frac{3}{2}n_p\psi_f \hat{I}_{\alpha\beta} - B\hat{\omega}\right) + h_{\omega_1}\tilde{i}_\alpha + h_{\omega_2}\tilde{i}_\beta \tag{14}$$

in which $\hat{I}_{\alpha\beta} = \hat{i}_\beta \cos(n_p\theta) - \hat{i}_\alpha \sin(n_p\theta)$, h_{ω_1} and h_{ω_2} are gains of feedback errors, which are defined as $\tilde{i}_\alpha = i_\alpha - \hat{i}_\alpha$ and $\tilde{i}_\beta = i_\beta - \hat{i}_\beta$.

C. CONVERGENCE ANALYSIS OF SPEED OBSERVER

According to Eqs. (5) and (6), the closed-loop current observer is designed as Eq. (15) with the output error feedback part.

$$\begin{bmatrix} L\dot{\hat{i}}_\alpha \\ L\dot{\hat{i}}_\beta \end{bmatrix} = \begin{bmatrix} u_\alpha \\ u_\beta \end{bmatrix} - R\begin{bmatrix} \hat{i}_\alpha \\ \hat{i}_\beta \end{bmatrix} + H\begin{bmatrix} \tilde{i}_\alpha \\ \tilde{i}_\beta \end{bmatrix} - n_p\omega\psi_f\begin{bmatrix} \cos\left(n_p\hat{\theta}\right) \\ \sin\left(n_p\hat{\theta}\right) \end{bmatrix} \quad (15)$$

where $\tilde{i}_\alpha = i_\alpha - \tilde{i}_\alpha$, $\tilde{i}_\beta = i_\beta - \tilde{i}_\beta$, $H = \begin{bmatrix} h_1 & 0 \\ 0 & h_2 \end{bmatrix}$ and $R = \begin{bmatrix} R_s & 0 \\ 0 & R_s \end{bmatrix}$.

Furthermore, with the consideration of the parameter errors generated in the process of stator resistance identification, the following error-model of currents are proposed.

$$\begin{bmatrix} L\dot{\tilde{i}}_\alpha \\ L\dot{\tilde{i}}_\beta \end{bmatrix} = \hat{R}\begin{bmatrix} \hat{i}_\alpha \\ \hat{i}_\beta \end{bmatrix} - R\begin{bmatrix} i_\alpha \\ i_\beta \end{bmatrix} - H\begin{bmatrix} \tilde{i}_\alpha \\ \tilde{i}_\beta \end{bmatrix} - n_p\omega\psi_f C \quad (16)$$

in which $C = \begin{bmatrix} -2\sin\frac{n_p\left(\theta+\hat{\theta}\right)}{2}\sin\frac{n_p\left(\theta-\hat{\theta}\right)}{2} \\ 2\cos\frac{n_p\left(\theta+\hat{\theta}\right)}{2}\sin\frac{n_p\left(\theta-\hat{\theta}\right)}{2} \end{bmatrix}$ and $\hat{R} = \begin{bmatrix} \hat{R}_s & 0 \\ 0 & \hat{R}_s \end{bmatrix}$.

When measurement of the rotor position is accurate enough, i.e., $\theta_m \to \theta$, it can be contained that $\sin\frac{n_p(\theta-\theta_m)}{2} \to 0$ [42]. Therefore, the linearization approximation can be expressed by following Eq. (17).

$$\begin{bmatrix} \dot{\tilde{i}}_\alpha \\ \dot{\tilde{i}}_\beta \end{bmatrix} = -\frac{1}{L}\begin{bmatrix} \tilde{R}_s & 0 \\ 0 & \tilde{R}_s \end{bmatrix}\begin{bmatrix} \hat{i}_\alpha \\ \hat{i}_\beta \end{bmatrix} - \begin{bmatrix} k_1 & 0 \\ 0 & k_2 \end{bmatrix}\begin{bmatrix} \tilde{i}_\alpha \\ \tilde{i}_\beta \end{bmatrix} \quad (17)$$

where $\tilde{R}_s = R_s - \hat{R}_s$, $k_1 = (R_s + h_1)/L$ and $k_2 = (R_s + h_2)/L$.

A positive definite function is structured.

$$V = \frac{1}{2}(L\tilde{i}_\alpha^2 + L\tilde{i}_\beta^2 + \tilde{R}_s^2) \quad (18)$$

The first derivative of Eq. (19) is defined as follows.

$$\dot{V} = L\left(\dot{\tilde{i}}_\alpha\tilde{i}_\alpha + \dot{\tilde{i}}_\beta\tilde{i}_\beta\right) + \left(\dot{R}_s - \dot{\hat{R}}_s\right)\tilde{R}_s \quad (19)$$

Since the actual stator resistance is a long-time varied parameter with small variation, R_s can be regarded as a constant, i.e., $\frac{dR_s}{dt} = 0$. Thus, this paper proposes an approximation as follows.

$$\dot{V} = -L\left(k_1\tilde{i}_\alpha^2 + k_2\tilde{i}_\beta^2\right) - \tilde{R}_s\left(\hat{i}_\alpha\tilde{i}_\alpha + \hat{i}_\beta\tilde{i}_\beta + \dot{\hat{R}}_s\right) \quad (20)$$

To eliminate the influence caused by the stator resistance parameter errors, the following resistance observer is proposed [43].

$$\dot{\hat{R}}_s = -\hat{i}_\alpha\tilde{i}_\alpha + \hat{i}_\beta\tilde{i}_\beta \quad (21)$$

In practice, the value of inductance L_2 is positive, so that $\dot{V}$ is a negative definite function when h_1 and h_2 are chosen as $h_1 > -\frac{R_s}{L_2}$ and $h_2 > -\frac{R_s}{L_2}$, or k_1 and k_2 are chosen as $k_1 > 0$, $k_2 > 0$. Therefore, according to the Lyapunov stability criterion, the current error equation described by Eq. (19) can converge asymptotically with reasonable output error feedback gain, and the design of resistance observer described by Eq. (22). Namely, $\lim_{t\to\infty}\left[\tilde{i}_\alpha(t)\right] = \lim_{t\to\infty}\left[\tilde{i}_\beta(t)\right] = 0$.

According to the Eqs. (13) and (14), the error of speed observed value is expressed as follows.

$$\dot{\tilde{\omega}} = -\frac{B}{J}\tilde{\omega} - \left[\frac{3}{2J}n_p\psi_f\sin\left(n_p\theta\right) + h_{\omega_1}\right]\tilde{i}_\alpha - \left[\frac{3}{2J}n_p\psi_f\cos\left(n_p\theta\right) + h_{\omega_2}\right]\tilde{i}_\beta \quad (22)$$

where $\tilde{\omega} = \omega - \hat{\omega}$. The equation $\lim_{t\to\infty}\left(\dot{\tilde{\omega}} + \frac{B}{J}\tilde{\omega}\right) = 0$ can be obtained when $t \to \infty$.

It is easy to prove $\lim_{t\to\infty}\tilde{\omega} = 0$ by the anti-evidence method. Therefore, the speed observer designed in this paper is convergent. Generally speaking, the ideal speed sensorless technology is introduced without rotor position sensor. This paper attempts to use the integral of the speed signal as the observation of rotor electrical angle, which can further test the convergence of the speed observer and whether the sensorless scheme based on the speed observer can be used.

D. SPEED CONTROLLER BASED ON ADRC

Based on one-dimensional sate variable x to estimate lumped disturbance of system, the system can be written in the form of single input and single output as follows.

$$\begin{cases} \dot{x} = f(x,t) + d(t) + bu(t) \\ y = x \end{cases} \quad (23)$$

where $f(x,t)$ is an unknown function, $d(t)$ represents external disturbances, b is a control gain, $u(t)$ is a control input signal, y is an output signal, and x is a system state variable

A typical second-order linear ADRC without model information can be designed as Eq. (24).

$$\begin{cases} \begin{bmatrix} \dot{z}_1 \\ \dot{z}_2 \end{bmatrix} = I\begin{bmatrix} z_1 \\ z_2 \end{bmatrix} + \begin{bmatrix} b \\ 0 \end{bmatrix}u(t) - \begin{bmatrix} 2p_r & 0 \\ 0 & p_r^2 \end{bmatrix}[z_1 - x(t)] \\ u(t) = k(v - z_1) - \frac{z_2}{b} \end{cases} \quad (24)$$

With the matrix $I = \begin{bmatrix} 0 & 0 \\ 0 & 1 \end{bmatrix}$, the parameter z_1 is the estimate of system state x; z_2 tracks the lumped disturbance $a_0(t)$ of the system, v is the input of controller, $u(t)$ is the control variable output from controller, and p_r is desired double pole. It is worth noting that $a_0(t)$ including the unknown system model information, the external disturbance and so on, i.e., $a_0(t) = f(x,t) + d(t)$. In addition, v is desired value of the state variable x in this paper.

When the system model is known accurately, the model information can be used to reduce the estimation burden of ESO and improve the anti-disturbance ability of the system. In this system, the state variables are chosen as follows.

$$\begin{cases} x_1 = x \\ x_2 = a(t) = f(x,t) - f_0\left(\hat{x},t\right) + d(t) \end{cases} \quad (25)$$

where $f_0(\hat{x}, t)$ is a namely model based on the operation mechanism of system, $\hat{x}$ is the estimation of x and the new lumped disturbance $a(t)$ of system includes observation error of system state variables, modeling error and external disturbance, etc..

Accordingly, the design of controller is adjusted as follows.

$$\begin{cases} \begin{bmatrix} \dot{z}_1 \\ \dot{z}_2 \end{bmatrix} = \mathrm{I}\begin{bmatrix} z_1 \\ z_2 \end{bmatrix} + \begin{bmatrix} b \\ 0 \end{bmatrix} u(t) + \begin{bmatrix} 1 \\ 0 \end{bmatrix} f_0(\hat{x}, t) \\ \qquad - \begin{bmatrix} 2p_r & 0 \\ 0 & p_r^2 \end{bmatrix} e_o \\ u(t) = k(v - z_1) - \dfrac{1}{b}\{z_2 + f(x, t)\} \end{cases} \tag{26}$$

where $e_o = z_1 - x(t)$.

In fact, the model information can be regarded as the known part of $a_0(t)$ to participate in the construction of controller. Moreover, $a_0(t)$ can be obtained based on the superposition of model information and observed disturbance $a(t)$ to compensate the disturbance of the control quantity. In compound schemes based on ADRC, ω is chosen as the one-dimensional sate variable x, ω_r is chosen as the input of speed controllers.

The model of wind turbine dynamics in $d - q$ coordinate system can be expressed as follows.

$$\dot{\omega} = \left[f(\omega, J, T_{tur}) + \left(b - \hat{b}\right) i_q\right] + \hat{b} i_q \tag{27}$$

in which $f(\omega_r, J, T_m) = \frac{1}{J}(T_m - B\omega_r)$, $b = -\frac{3}{2J} n_p \psi_f$, and $\hat{b}$ is the estimation of b.

According to (26), the speed controller independent of model information can be designed as follows.

$$\begin{cases} \dot{z}_1 = z_2 - 2p_r(z_1 - \omega) + \hat{b} u(t) \\ \dot{z}_2 = p_r^2(z_1 - \omega) \\ u(t) = k(\omega_r - z_1) - z_2/\hat{b} \end{cases} \tag{28}$$

where the actual meaning of lumped disturbance $a_0(t)$ can be expressed as follows.

$$z_2 \to a_0(t) = \frac{1}{J}(T_{tur} - B\omega_r) + \left(b - \hat{b}\right) i_q \tag{29}$$

Another form of the mathematical model can be given as follows.

$$\dot{\omega} = f_0\left(\hat{\omega}, \hat{J}, \hat{T}_{tur}\right) + a(t) + \hat{b} i_q \tag{30}$$

And the actual meaning of lumped disturbance $a(t)$ have changed as follows.

$$z_2 \to a(t) = f(\omega, J, T_{tur}) - f_0\left(\hat{\omega}, \hat{J}, \hat{T}_{tur}\right) + \left(b - \hat{b}\right) i_q \tag{31}$$

where $\hat{\omega}_r$, $\hat{J}$ and $\hat{T}_m$ are the measurements of wind turbine speed, system inertia, and driving torque output by wind wheel, respectively. The equation of $f_0\left(\hat{\omega}, \hat{J}, \hat{T}_m\right) = \frac{1}{\hat{J}}\left(\hat{T}_m - B\hat{\omega}\right)$ is the namely model expressed by $f_0(\hat{x}, t)$ in ADRC, and $f(\omega, J, T_m)$ is the real dynamical model of wind turbine with the characteristics of a nonlinear, strongly coupled multilevel system.

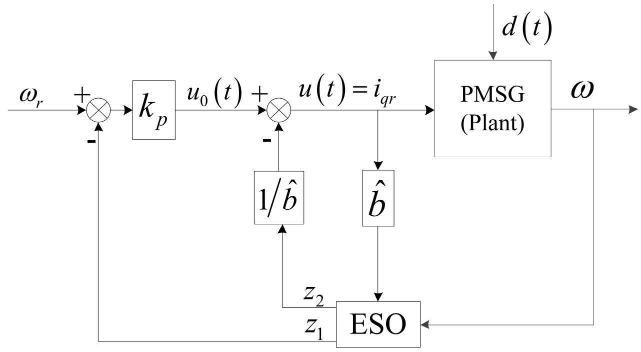

FIGURE 3. The structure of typical ADRC.

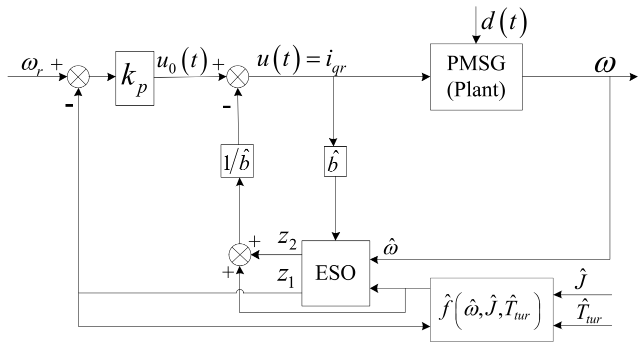

FIGURE 4. The structure of model-assisted ADRC.

Moreover, the speed controller with assistance of model information designed according to (28) can be given as following Eq. (32).

$$\begin{cases} \dot{z}_1 = z_2 - 2p_r(z_1 - \omega) + f_0\left(\hat{\omega}, \hat{J}, \hat{T}_m\right) + \hat{b} u(t) \\ \dot{z}_2 = -p_r^2(z_1 - \omega) \\ u(t) = k_p(\omega_r - z_1) - \left[z_2 + f_0\left(\hat{\omega}, \hat{J}, \hat{T}_m\right)\right]/\hat{b} \end{cases} \tag{32}$$

To sum up, the structure of speed controller independent of model information is shown by Fig.3, and the structure of speed controller with assistance of model information is shown by Fig.4.

IV. SIMULATION AND ANALYSIS

A. SIMULATIONS OF WIND SPEED MODEL

The fluctuation, randomness and time-varying of wind speed make the output power of wind turbine fluctuate greatly, which makes the wind power system unable to adjust to the optimal energy conversion state quickly, and has a great influence on the safe operation of the power system. In order to simulate the actual wind field reasonably, the natural wind v_n is divided into four types: base wind v_b, gust wind v_g, slope wind v_r and random wind v_a, whose corresponding mathematical models are established according to the static, abrupt, gradual and random characteristics of wind field, respectively. Namely, $v_n = v_b + v_g + v_r + v_a$.

The base wind reflects the mean wind speed in wind field, which can be approximately assumed to be unchanged over a period of time. Therefore, this paper takes the base wind as $v_b = 6m/s$.

The gust wind reflects the large variation wind speed in wind field of gust wind, which can be approximately expressed by cosine function as Eq. (33). In this paper, the maximum speed G_m of gust wind is $2m/s$, the start time t_{g1} is *0.8s*, and the end time t_{g2} is *2.8s*.

$$v_g = \begin{cases} \frac{G_m}{2}\left[1-\cos\left(2\pi\frac{t-t_{g1}}{t_{g2}-t_{g1}}\right)\right], & t_{g1} \le t < t_{g2} \\ 0, & others \end{cases} \tag{33}$$

The sloping wind varies linearly in a certain period of time with finite non-differentiable points in the continuous time. In order to verify the influence of wind speed with different rates on the dynamic characteristics of WECS, multi-segment broken lines is proposed to simulate the sloping wind, whose maximum speed R_m is $2m/s$, first turn time t_{r1} is *0.8s*, second turn time t_{r2} is 2.2 s, third turn time t_{r3} is *2.8s*, fourth turn time t_{4r} is *3.2s*, and termination time t_{r5} is *3.6s*. In addition, the extension of the third segment of the broken line intersects the x axis at t^*_{r3}, which is taken as *3.35s*. The mathematical model of the sloping wind is as follows.

$$v_r = \begin{cases} R_m\left(1-\frac{t-t_{r1}}{t_{r1}-t_{r2}}\right), & t_{r1} \le t < t_{r2} \\ R_m, & t_{r2} \le t < t_{r3} \\ R_m\frac{t^*_{r3}-t}{t^*_{r3}-t_{r3}}, & t_{r3} \le t < t_{4r} \\ R_t\frac{t_{r5}-t}{t_{r5}-t_{4r}}, & t_{4r} \le t < t_{r5} \\ 0, & others \end{cases} \tag{34}$$

where $R_t = \frac{R_m(t^*_{r3}-t_{r4})}{t^*_{r3}-t_{r3}}$.

The noise wind is simulated by the combination of two random noise with uniform probability density, whose start time t_{n1} is *0.8s* and terminal time is *2.8s*. The mathematical model of the noise wind can be expressed as following equation [44].

$$v_a = \begin{cases} \frac{A_m}{2}U_i\cos\left[2\pi t+\varphi_i\right], & t_{n1} \le t \le t_{n2} \\ 0 & others \end{cases} \tag{35}$$

In Eq. (35), $U(i)$ denotes the random noise that obeys a uniform distribution on the interval $(0 \sim 1)$, φ_i denotes the random noise that obeys a uniform distribution on the interval $(0 \sim 2\pi)$, and A_m represents the maximum possible random wind speed.

Considering that the base wind always exists in the wind field, the dynamic performance of WECS is analyzed in the wind fields with superimposition of the base wind. To sum up, the variation trend of wind speed in different wind fields are shown in Fig.5.

B. SIMULATIONS RESULTS OF CONTROL SCHEME FOR WECS

In order to verify performance of the speed controllers based on ADRC proposed in **Section IV,** this paper constructs two sets of simulation platforms, based on Matlab/Simulink, according to the control structure proposed in Fig. 2. The wind turbines of systems are constructed according to the mathematical model described in Eqs. (1) $\sim$ (6) and (9) whose specific parameters are shown in Table 1, and the speed controllers are constructed according to the structures shown in Figs. 4 and 5.

In order to verify the effect of position sensor precision on the system, local fine tuning is carried out in the speed observer. The structure with precise rotor position sensor is called speed sensorless structure, and the structure with the integral of rotational speed signal as the rotor electrical angle is called the position sensorless structure. Combined with the WECS control schemes based on ADRC, the effects of two speed observer structures on the control performance are verified by simulation. The control parameters of different control schemes are shown in Tables 2 and 3. The observer control parameters are shown in Table 4. The rotational speed tracking effect of the speed rejection control scheme combined with speed sensorless technology is shown in Figs.6$\sim$9, and the simulation result of the position sensorless control scheme is shown in Figs.10$\sim$13. In addition, in the Figs. 6$\sim$13, $ADRC_r$represents the curve of reference speed for PMSG calculated by Eq. (3), *ADRC* and $ADRC_O$

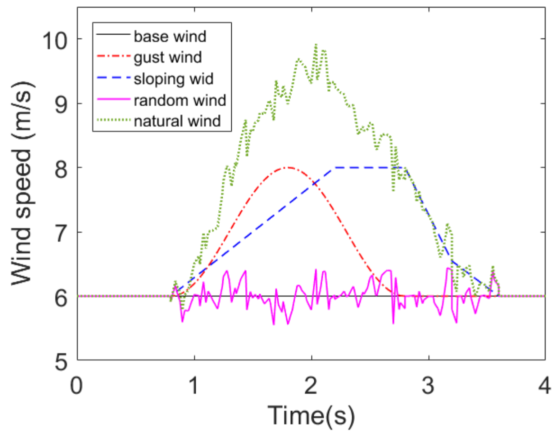

FIGURE 5. The curves of different wind types.

TABLE 1. Parameters of the wind turbine.

Rotor inertia(kg·m^2)	0.0027	Pole pairs	4
Permanent magnetic flux(Wb)	0.1194	Stator resistance(Ω)	0.0485
Stator inductance(H)	8.5×10^{-3}	Viscous damping	49.24×10^{-5}
Wind turbine parameters Air density(kg/m^3)	1.25	Turbine blade radius (m)	1.5
Optimum tip-speed ratio	8.1	Basic wind speed(m/s)	6

TABLE 2. Parameters for typical ADRC.

Parameters	Speed sensorless scheme	Position sensorless scheme
b	320	307
p	24	25
k_p	100	100

TABLE 3. **Parameters for model-assisted ADRC.**

Parameters	Speed sensorles scheme	Position sensorless scheme
b	307	302
p	32.4	34
k_p	100	100

TABLE 4. **Parameters for speed observer.**

Parameters	Speed sensorless scheme	Position sensorless scheme
h_1	1.2	1.4
h_2	1	1.4
$h_{\omega 1}$	20	15
$h_{\omega 2}$	20	15

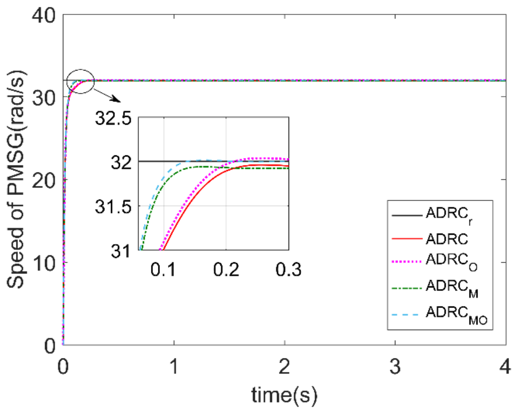

FIGURE 6. **The speed tracking without speed sensor in the base wind field.**

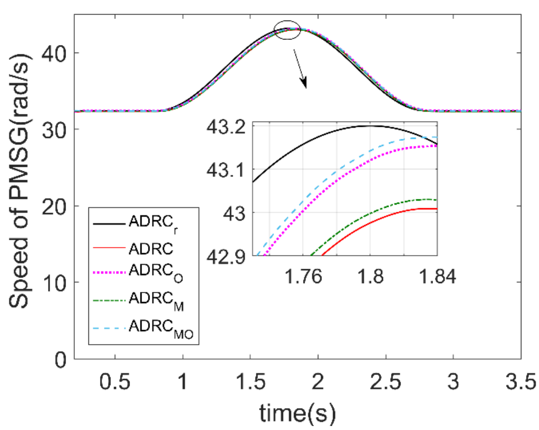

FIGURE 7. **The speed tracking without speed sensor in the gust wind field.**

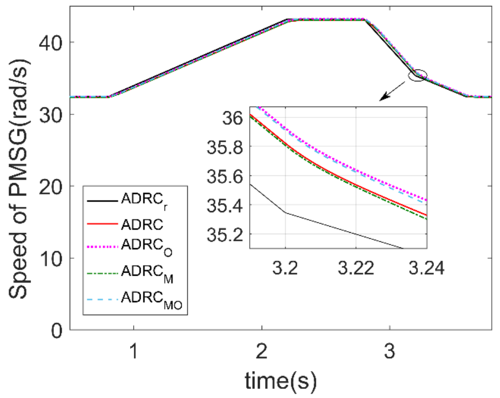

FIGURE 8. **The speed tracking without speed sensor in the sloping wind field.**

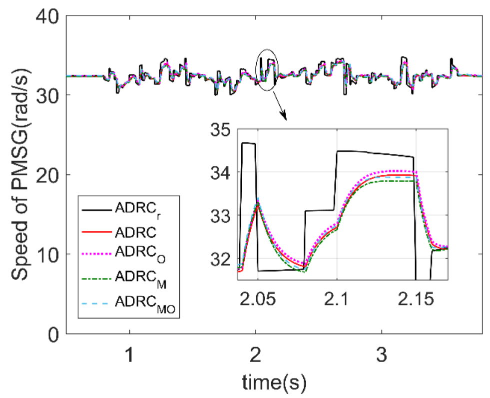

FIGURE 9. **The speed tracking without speed sensor in the random wind field.**

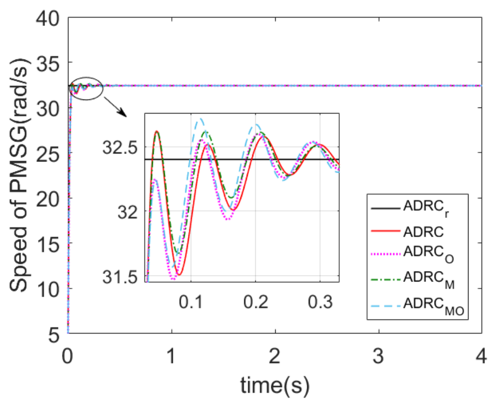

FIGURE 10. **The speed tracking without position sensor in the base wind field.**

represent the speed response curve and the observation speed curve of PMSG in the close-loop system with the typical ADRC scheme, $ADRC_M$ and $ADRC_{MO}$ represent the speed response curve and the observation speed curve of PMSG in the close-loop system with the model-assisted ADRC scheme.

It should be noted that the PMSG models of the simulation platforms adopts the mathematical model in $\alpha-\beta$ coordinate system, which not only accords with the causality law of coordinate transformation, but also matches the speed observer designed in this paper. If the mathematical model of PMSG in $d-q$ coordinate system and the speed observer in $\alpha-\beta$ coordinate system are used at the same time, not only the chattering will be caused by coordinate transformation, but also the observer gain will be increased by $3\sim4$ orders of magnitude.

C. PHENOMENON ANALYSIS

The Fig.6 shows that the speed observer proposed in this paper can track the wind turbine speed quickly even when the system works at low speed, which matches the assumption that the system runs below the rated speed. Therefore, even

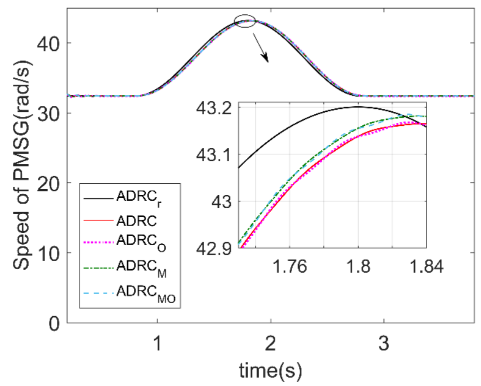

FIGURE 11. The speed tracking without position sensor in the gust wind field.

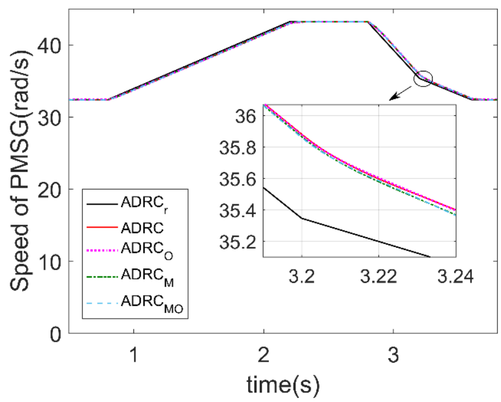

FIGURE 12. The speed tracking without position sensor in the sloping wind field.

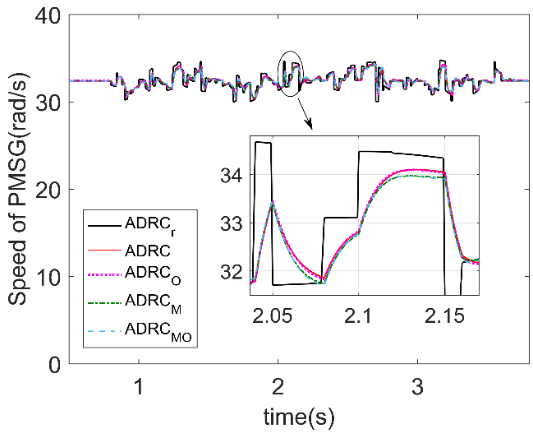

FIGURE 13. The speed tracking without position sensor in the random wind field.

in the case of low wind speed, the speed of wind turbine can be can effectively controlled without speed sensor. Besides, compared with the control scheme based on typical ADRC, the scheme based on model-assisted ADRC can track desired speed faster with less overshoot and smaller steady-state. In other words, the model-assisted ADRC has the advantages of stability and rapidity. The detailed controller performance indexes of two schemes and the steady state error of the observer are analyzed in Table 5.

TABLE 5. Performance indexes of typical ADRC and model-assisted ADRC.

Parameters	Overshoot (%)	Rise time (s)	Steady state errors	Steady observation errors
Typical ADRC	320	307	0.085	0.08
Model-assisted ADRC	24	25	0.084	0.08

TABLE 6. Absolute integral errors of speed tracking in random wind field.

IAE	Speed sensorless	Position sensorless
Typical ADRC	1800.1	1740.4
Model-assisted ADRC	1762.0	1709.3

TABLE 7. Absolute integral errors of speed observation in base wind field.

IAE	Typical ADRC	Model-assisted ADRC
Speed sensorless	216.5703	216.1776
Position sensorless	46.3122	46.1332

Moreover, the speed controller based on model-assisted ADRC can reflect the speed change trend more quickly so that it has a better speed tracking effect, which can be seen from figs.7 and 8. Unfortunately, this characteristic also leads to the special situation shown in Fig.9. Due to the inevitable delay of speed response, the wind turbine cannot track the desired speed in the shortest time. Therefore, when the trend of noise wind changes with a relatively large amplitude of variation, the quicker respond to the change trend of the model-assisted ADRC makes the response of rotor speed deviate prematurely from the ideal orbit, which seems no contribution to the improvement of speed tracking performance. However, on the other hand, this is more conducive to the stability of system. In order to further compare the overall performance of the two control schemes, the absolute integral errors (IAE) of speed tacking in the random wind field are compared as shown in Table 6, which proves that the model-assisted ADRC still has more advantages in long operation control of WECS.

In the simulation results shown in Figs.6∼8 and Table 5, the inevitable problem is that the speed tacking errors are greatly increased for the steady state error of the speed observer. In fact, the errors signal obtained by the speed controllers are the errors between the rotator speed observation and the desired speed, rather than the real speed error signal, so the speed control cannot completely eliminate the observation error. In theory, the problem can be solved by adjusting the structure of the speed controller or improving the accuracy of the speed observer.

In contrast to Figs.10∼13, it can be inferred that the observation error of rotational speed is mainly caused by the inaccuracy of position sensor. When the integral of rotor speed is used as the electrical angle observation, the steady state error problem of rotor speed observation can be solved well. This is because the design of the rotor speed observer introduces the current error signal to correct the deviation, which leads to the error correction for the rotor electrical angle observation. To further quantify the observed performance differences between speed sensorless structure and position sensorless structure of speed observer, Table 7 gives the IAE of the rotor speed observations under different control schemes in base wind field.

Unfortunately, as the extreme case shown in Fig.10, the oscillation phenomenon appears on the speed response of wind turbine when the step signal appears. However, in this case, the actual speed variation of the model-assisted ADRC scheme shows a more stable convergence trend and converges at a faster speed to the desired speed, i.e., it is less affected by the fluctuation of the rotational speed observation signal. In contrast, since the model information obtained by the speed controller is less, the disturbance estimation of the typical ADRC is more susceptible to the fluctuation of the observed signal, and the convergence trend of the rotor speed is fluctuated.

Finally, the Figs.11∼13 show that the speed controller has better speed tracking performance when the rotor speed observation is more accurate. Moreover, the variation tendency of speed tracking is basically consistent with the results in Figs.7∼8, which is not worth repeating.

V. CONCLUSION

In this paper, the model information is introduced into the typical ADRC, and the new controller structure is applied to the WECS. The performance differences between the typical ADRC and model-assisted ADRC are compared by simulations, and their respective advantages are analyzed. In addition, on the basis of speed observer design and convergence analysis, a position sensorless speed observer structure is proposed in this paper. The convergence of the original speed observer is further verified by simulation. Furthermore, the simulation results show that the position sensorless speed observer structure has higher observation accuracy.

REFERENCES

[1] T. R. S. DeFreitas, P. J. M. Menegaz, and D. S. L. Simonetti, ''Rectifier topologies for permanent magnet synchronous generator on wind energy conversion systems: A review,'' *Renew. Sustain. Energy Rev.*, vol. 54, pp. 1334–1344, Aug. 2013.

[2] X. Li, C. Xie, S. Quan, L. Huang, and W. Fang, ''Energy management strategy of thermoelectric generation for localized air conditioners in commercial vehicles based on 48?V electrical system,'' *Appl. Energy*, vol. 231, pp. 887–900, Dec. 2018.

[3] L. Sun, Y. Jin, L. Pan, J. Shen, and K. Y. Lee, ''Efficiency analysis and control of a grid-connected pem fuel cell in distributed generation,'' *Energy Convers. Manage.*, vol. 195, pp. 587–596, Sep. 2019.

[4] S. Q. Li, K. Zhang, J. Li, and C. Liu, ''On the rejection of internal and external disturbances in a wind energy conversion system with direct-driven PMSG,'' *ISA Trans.*, vol. 61, no. 3, pp. 95–103, Mar. 2016.

[5] D. Kumar and K. Chatterjee, ''A review of conventional and advanced MPPT algorithms for wind energy systems,'' *Renew. Sustain. Energy Rev.*, vol. 55, pp. 957–970, Mar. 2016.

[6] Y. Zhao, C. Wei, Z. Zhang, and W. Qiao, ''A review on position/speed sensorless control for permanent-magnet synchronous machine-based wind energy conversion systems,'' *IEEE J. Emerg. Sel. Topics Power Electron.*, vol. 1, no. 4, pp. 203–216, Dec. 2013.

[7] X. Zeng, T. Liu, S. Wang, Y. Dong, and Z. Chen, ''Comprehensive coordinated control strategy of PMSG-based wind turbine for providing frequency regulation services,'' *IEEE Access*, vol. 7, pp. 63944–63953, 2019.

[8] N. D. Dao, D.-C. Lee, and S. Lee, ''A simple and robust sensorless control based on stator current vector for PMSG wind power systems,'' *IEEE Access*, vol. 7, pp. 8070–8080, 2019.

[9] S. Li, T. A. Haskew, and L. Xu, ''Conventional and novel control designs for direct driven PMSG wind turbines,'' *Electr. Power Syst. Res.*, vol. 80, pp. 328–338, Mar. 2010.

[10] Y. She, X. She, and M. E. Baran, ''Universal tracking control of wind conversion system for purpose of maximum power acquisition under hierarchical control structure,'' *IEEE Trans. Energy Convers.*, vol. 26, no. 3, pp. 766–775, Sep. 2011.

[11] F. Jaramillo-Lopez, G. Kenne, and F. Lamnabhi-Lagarrigue, ''A novel online training neural network-based algorithm for wind speed estimation and adaptive control of PMSG wind turbine system for maximum power extraction,'' *Renew. Energy*, vol. 86, pp. 38–48, Feb. 2016.

[12] Z. Q. Wu, W. J. Jia, and C. H. Wu, ''Maximum wind power tracking based on cloud RBF neural network,'' *Renew. Energy*, vol. 86, pp. 466–472, Feb. 2016.

[13] Das and B. Subudhi, ''A H∞ robust active and reactive power control scheme for a PMSG-based wind energy conversion system,'' *IEEE Trans. Energy Convers.*, vol. 33, no. 3, pp. 980–990, Sep. 2018.

[14] Y. Gui, C. Kim, and C. C. Chung, ''Improved low-voltage ride through capability for PMSG wind turbine based on port-controlled Hamiltonian system,'' *Int. J. Control Automat. Syst.*, vol. 14, no. 5, pp. 1195–1204, 2016.

[15] H. X. Wang, J. Yang, Z. Chen, W. Ge, Y. Ma, Z. Xing, and L. Yang, ''Model predictive control of PMSG-based wind turbines for frequency regulation in an isolated grid,'' *IEEE Trans. Ind. Appl.*, vol. 54, no. 4, pp. 3077–3089, Jun. 2018.

[16] M. Ayadi and N. Derbel, ''Nonliear adaptive backstepping control for variable-speed wind energy conversion system-based permanent magnet synchronous generator,'' *Int. J. Adv. Manuf. Technol.*, vol. 92, nos. 1–4, pp. 39–46, 2017.

[17] S. M. Mozayan, M. Saad, H. Vahedi, H. Fortin-Blanchette, and M. Soltani, ''Sliding mode control of PMSG wind turbine based on enhanced exponential reaching law,'' *IEEE Trans. Ind. Electron.*, vol. 63, no. 10, pp. 6148–6159, Oct. 2016.

[18] B. Yang, T. Yu, H. Shu, Y. Zhang, J. Chen, Y. Sang, and L. Jiang, ''Passivity-based sliding-mode control design for optimal power extraction of a PMSG based variable speed wind turbine,'' *Renew. Energy*, vol. 119, pp. 577–589, Apr. 2018.

[19] K. Ohnishi, M. Nakao, and K. Miyachi, ''Microprocessor controlled DC motor for load-insensitive position servo systems,'' *IEEE Trans. Ind. Electron.*, vol. IE-34, no. 1, pp. 44–49, Feb. 1987.

[20] C.-M. Hong, C.-H. Chen, and C.-S. Tu, ''Maximum power point tracking-based control algorithm for PMSG wind generation system without mechanical sensors,'' *Energy Convers. Manage.*, vol. 69, pp. 58–67, May 2013.

[21] M. Abdelrahem, C. M. Hackl, Z. Zhang, and R. Kennel, ''Robust predictive control for direct-driven surface-mounted permanent-magnet synchronous generators without mechanical sensors,'' *IEEE Trans. Energy Convers.*, vol. 33, no. 1, pp. 179–189, Aug. 2018.

[22] R. Errouissi, A. AI-Durra, and M. Debouza, ''A novel design of PI current controller for PMSG-based wind turbine considering transient performance specifications and control saturation,'' *IEEE Trans. Ind. Electron.*, vol. 65, no. 11, pp. 8624–8634, Nov. 2018.

[23] S.-K. Kim and K.-B. Lee, ''Robust offset-free speed tracking controller of permanent magnet synchronous generator for wind power generation applications,'' *Electronics*, vol. 7, no. 4, pp. 1–13, 2018.

[24] T. Yang, N. Sun, H. Chen, and Y. Fang, ''Neural network-based adaptive antiswing control of an underactuated ship-mounted crane with roll motions and input dead zones,'' *IEEE Trans. Neural Netw. Learn. Syst.*, to be published. doi: 10.1109/TNNLS.2019.2910580.

[25] J. Han, ''A class of extended state observers for uncertain systems,'' *Control Decis.*, vol. 10, no. 1, pp. 85–88, 1995.

[26] J. Han, ''From PID to active disturbance rejection control,'' *IEEE Trans. Ind. Electron.*, vol. 56, no. 3, pp. 900–906, Mar. 2009.

[27] Z. Gao, ''Scaling and bandwidth parameterization based controller tuning,'' in *Proc. Amer. Control Conf.*, Denver, CO, USA, Jun. 2003, pp. 96–4989.

[28] S. Q. Li and J. Li, "Output predictor-based active disturbance rejection control for a wind energy conversion system with PMSG," *IEEE Access*, vol. 5, pp. 5205–5214, 2017.
[29] Y. Xu and S. Zhao, "Mitigation of subsynchronous resonance in series-compensated DFIG wind farm using active disturbance rejection control," *IEEE Access*, vol. 7, pp. 68812–68822, 2019.
[30] D. K. Sagiraju, O. Yeddulapeda, and S. B. Choppavarapu, "A new control approach to improve the dynamic performance and ride through capability of PMSG wind energy system," *J. Renew. Sustain. Energy*, vol. 10, no. 4, 2018, Art. no. 043310.
[31] Q. Shi, G. Wang, L. Fu, Y. Liu, Y. Wu, and L. Xu, "Virtual inertia control of D-PMSG based on the principle of active disturbance rejection control," *J. Elect. Eng. Technol.*, vol. 10, no. 5, pp. 1969–1982, 2015.
[32] Y. Ma, J. Liu, H. Liu, and S. Zhao, "Active-reactive additional damping control of a doubly-fed induction generator based on active disturbance rejection control," *Energies*, vol. 11, no. 5, p. 1314, 2018.
[33] Y. Tang, Y. Bai, C. Huang, and B. Du, "Linear active disturbance rejection-based load frequency control concerning high penetration of wind energy," *Energy Convers. Manage.*, vol. 95, pp. 259–271, May 2015.
[34] L. Sun, J. Shen, Q. Hua, and K. Y. Lee, "Data-driven oxygen excess ratio control for proton exchange membrane fuel cell," *Appl. Energy*, vol. 231, pp. 866–875, Dec. 2018.
[35] N. Sun, D. Liang, Y. Wu, Y. Chen, Y. Qin, and Y. Fang, "Adaptive control for pneumatic artificial muscle systems with parametric uncertainties and unidirectional input constraints," *IEEE Trans. Ind. Inform.*, to be published. doi: 10.1109/TII.2019.2923715.
[36] R. Aubree, F. Auger, M. Macé, and L. Loron, "Design of an efficient small wind-energy conversion system with an adaptive sensorless MPPT strategy," *Renew. Energy*, vol. 86, pp. 280–291, Feb. 2016.
[37] H. Yang, Y. Zhang, P. D. Walker, N. Zhang, and B. Xia, "A method to start rotating induction motor based on speed sensorless model-predictive control," *IEEE Trans. Energy Convers.*, vol. 32, no. 1, pp. 359–368, Sep. 2016.
[38] S. S. Yu, G. Zhang, T. Fernando, and H. H. Iu, "A DSE-based SMC method of sensorless DFIG wind turbines connected to power grids for energy extraction and power quality enhancement," *IEEE Access*, vol. 8, pp. 76596–76605, 2018.
[39] J. Yan, H. Lin, Y. Feng, X. Guo, Y. Huang, and Z. Q. Zhu, "Improved sliding mode model reference adaptive system speed observer for fuzzy control of direct-drive permanent magnet synchronous generator wind power generation system," *IET Renew. Power Gener.*, vol. 7, no. 1, pp. 28–35, Feb. 2013.
[40] D. Song, J. Yang, M. Dong, and Y. H. Joo, "Kalman filter-based wind speed estimation for wind turbine control," *Int. J. Control Automat. Syst.*, vol. 15, no. 3, pp. 1089–1096, 2017.
[41] Z. Zhang, Y. Zhao, W. Qiao, and L. Qu, "A space-vector-modulated sensorless direct-torque control for direct-drive PMSG wind turbines," *IEEE Trans. Ind. Appl.*, vol. 50, no. 4, pp. 2331–2341, Jun. 2014.
[42] A. Urtasun, P. Sanchis, and L. Marroyo, "Small wind turbine sensorless MPPT: Robustness analysis and lossless approach," *IEEE Trans. Ind. Appl.*, vol. 50, no. 6, pp. 4113–4121, Dec. 2014.
[43] G. Foo and M. F. Rahman, "Sensorless direct torque and flux-controlled IPM synchronous motor drive at very low speed without signal injection," *IEEE Trans. Ind. Electron.*, vol. 57, no. 1, pp. 395–403, May 2010.
[44] T. Gao, Y. J. Liu, L. Liu, and D. Li, "Adaptive neural network-based control for a class of nonlinear pure-feedback systems with time-varying full state constraints," *IEEE/CAA J. Automatica Sinica*, vol. 5, no. 5, pp. 923–933, Jul. 2018.

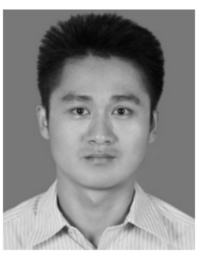

SHENGQUAN LI was born in Changde, China, in 1982. He received the Ph.D. degree in mechatronics from the Nanjing University of Aeronautics and Astronautics, Nanjing, China, in 2012. From September 2014 to March 2015, he was a Research Assistant with the Department of Automatic Control and Systems Engineering, The University of Sheffield, U.K. Since 2012, he has been with Yangzhou University, China, where he is currently an Associate Professor and a Doctoral Supervisor. His current research interests include disturbance estimation theories and their applications to renewable energy systems and piezoelectric structural vibration suppression. He has served on the Technical Program Committee for several international conferences, including the IEEE CYBER 2018 and ICONIP2018.

MENGYING CAO was born in Xuyi, China, in 1996. She received the B.S. degree from the School of Hydraulic, Energy and Power Engineering, Yangzhou University, China, in 2018. She is currently pursuing the degree with the School of Automation, Southeast University. Her main research interests include anti-disturbance methods and their applications to wind energy conversion systems and high-precision servo systems.

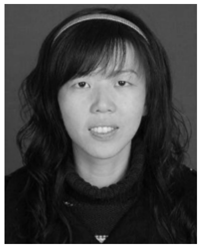

JUAN LI was born in Linyi, China, in 1983. She received the B.S. degree from the Department of Automatic Control, Weifang University, Weifang, China, in 2006, the M.S. degree from the School of Automation, Anhui University of Technology, Maanshan, China, in 2009, and the Ph.D. degree from the School of Automation, Southeast University, Nanjing, China, in 2013. She is currently an Associate Professor with the School of Hydraulic, Energy and Power Engineering, Yangzhou University. Her main research interest includes active anti-disturbance control.

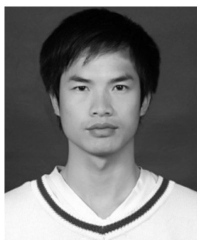

JIUFA CAO was born in Ninghua, Fujian, China, in 1986. He received the Ph.D. degree in mechatronics from the Nanjing University of Aeronautics and Astronautics, Nanjing, China, in 2015. From January 2015 to July 2015, he was a Visiting Researcher with the Department of Mechanical Engineering, The University of Sheffield, U.K. Since 2016, he has been with Yangzhou University, China, where he is currently a Lecturer and a Master Supervisor. His current research interests include wind turbine aerodynamics, wind turbine control, and their applications to renewable energy systems.

ZHONGWEI LIN was born in Yantai, China, in 1981. He received the B.E. and M.E. degrees from the Shandong University of Science and Technology, in 2004 and 2007, respectively, and the Ph.D. degree from the Beijing University of Aeronautics and Astronautics, in 2011. He is currently an Associate Professor with the School of Control and Computer Engineering, North China Electric Power University, Beijing. His research interests include wind turbine modeling and control, wind farm control, stochastic control, and nonlinear control.